Ladislav KNEBL[1], Nicola BIANCHI[2], Giacomo BACCO[2], Cestmir ONDRUSEK[1]

Brno University of Technology, Czech Republic (1), University of Padova, Italy (2)

doi:10.15199/48.2020.01.24

Synchronous Reluctance Motor Analytical Model Cross-saturation and Magnetization Analysis

Abstract.
The synchronous reluctance motor design process is usually considering objectives that are in direct or indirect relationship with the rotor magnetic saliency ξ. The magnetic saliency is defined as the ratio of direct (d) L_d and quadrature (q) inductances L_q. Both inductances and their dependence on the dq-axis current plane are investigated with a non-linear analytical model in this paper. With the non-linear analytical model linked to the analysis procedures is also possible to determine the synchronous reluctance motor cross-saturation effect.

Streszczenie. *W artykule analizowano asymetrię magnetyczną (saliency) wirnika silnika reluktancyjnego. Zastosowano model nieliniowy uwzględniający tę asymetrię i umożliwiający określenie efektu nasycenia.* ***Analityczny model silnika reluktancyjnego uwzględnmiający asymetrię magnetyczną i nasycenie rdzenia.***

Keywords: Synchronous reluctance machine, Non-linear analytical model, Finite element analysis, Magnetic flux.
Słowa kluczowe: synchroniczny silnik reluktancyjny, model nieliniowy, asymetria magnetyczna

Table 1: SynRel machine specifications

Parameter	Symbol	Value
Stator outer diameter	D_o	200 mm
Stator inner diameter	D	125 mm
Stack length	L_{stk}	40 mm
Air gap length	g	0.3 mm
Number of slots	Q_s	36
Number of poles	2p	4

Introduction

The Synchronous Reluctance (SynRel) machines are usually designed or analyzed by Finite Element Analysis (FEA) [1, 2]. The Reluctance Network (RN) method is the first alternative to FEA. The RN benefits from the rapid estimation of motor characteristics and optimization [3]. The last commonly used method is Analytical Model (AM), used for instance to minimize the torque ripple in [4]. In [5] a combination of both AM and FEA method for optimization of a permanent magnet assisted SynRel is proposed, which yields to a good compromise between speed and precision.
The AM significance has been presented in various papers[6, 7, 8]. The AM role in design process moved from the quick simple torque and torque ripple estimation into more sophisticated tool. The AM was mostly used to the torque and performance analysis and ripple reduction [4, 9, 10] and rarely extended for the iron losses estimation [11, 12]. Usually satisfactory results are found compared to FEA, as in [12].
The non-linear AM used in this paper is very similar to the one described in [12] and is used for further analysis. The purpose is to provide more thorough analysis of the proposed AM and compare it to FEA, while keeping the advantage of the AM, that is the short estimation time. In particular, the cross-saturation effect and the limit torque-speed characteristic are derived and studied.

Analytical model

The machine under study is a previously optimized SynRel machine, for torque ripple reduction, with the integral-slot winding and transversally laminated rotor. The key parameters of the machine under study are listed in Table 1. Fig. 1 shows the cross section area of the SynRel motor, where the direct (d) and quadrature (q) axis are highlighted.

Since the magnetic ribs are highly saturated, they can be removed in AM to simplify the solved magnetic circuit. In

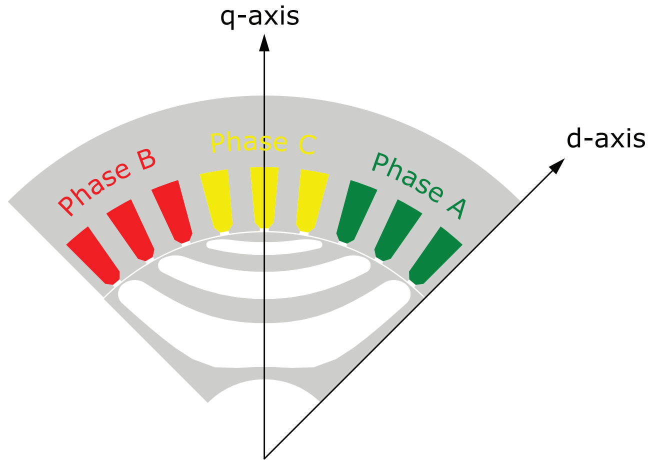

Fig. 1: Cross section of the analyzed motor with d- and q-axis alignment

order to correctly compare FEA and AM results, it is necessary to cut out the end of the flux barriers as depicted in Fig. 2. The flux barrier ends are cut out to minimize the saturation effect of the end barrier ribs, that are not included in the analytical model. In case of PM assisted SynRel machines, such ribs are saturated by the PM flux. Practically, a part of the PM flux is lost for such saturation. Nonetheless, the accuracy of the solution is just slightly modified.

The analytical model is based on the winding function theory, for which the electric loading is:

$$K_s(\theta_r) = \sum_{\nu} \hat{K_\nu} \sin\left[\nu p \theta_r + (\nu - 1)\omega_m^e t - \alpha_i^e\right] \tag{1}$$

where ν is the harmonic order, $\hat{K_\nu}$ is the peak of the electric loading of ν-th harmonic, p is the number of pole pairs, θ_r is the coordinate angle in the rotor reference frame, ω_m^e is the speed in radians per second and α_i^e is the current angle in electrical degrees. The stator electric potential in the rotor reference frame (angle θ_r is used) can be estimated as:

$$U_s(\theta_r) = \int K_s(\theta_r)\frac{D}{2}d\theta_r \tag{2}$$

The flux density can be derived by

$$B_g(\theta_r) = \mu_0 \frac{-U_s(\theta_r) + U_r(\theta_r)}{g} \tag{3}$$

where μ_0 is the vacuum permeability and $U_r(\theta_r)$ is the rotor

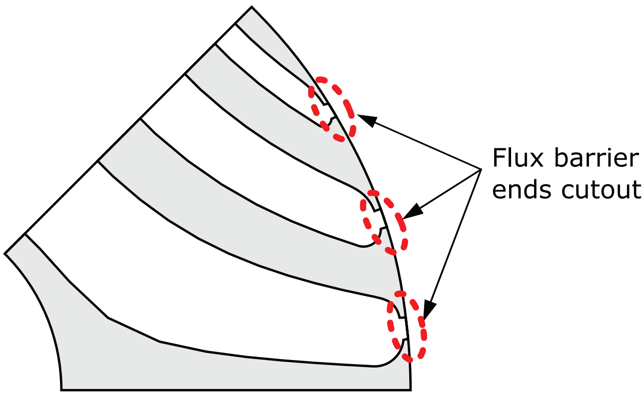

Fig. 2: Flux barrier cutouts (width of cutouts is exaggerated)

magnetic potential. The torque can be calculated from the Lorentz force density according to

$$T_m = -\frac{D}{2}\int_0^{2\pi} B_g(\theta_r)U_r(\theta_r)\frac{DL_{stk}}{2}d\theta_r \tag{4}$$

The magnetic voltage drops are considered in the AM. The saturation factor is defined as the magnetic voltage drop along the total path including stator and rotor iron divided by the magnetic voltage drop in the air gap:

$$k_{sat} = \frac{\Psi_{tot}}{\Psi_g} \tag{5}$$

This factor is considered as an index of convergence of the non-linear field problem. The error is estimated as

$$err = \|k_{sat}^{n+1} - k_{sat}^{n}\| \tag{6}$$

A random relaxation factor to improve the convergence is defined as:

$$k_{sat}^{n+1} = k_{sat}^{n} + 0.5\,\text{rand}\,(k_{sat}^{n+1} - k_{sat}^{n}) \tag{7}$$

where n is the number of iterations. A random relaxation factor delivered occasional faulty behavior, the solution of which is discussed in the Appendix.

Flux linkage calculation methods

There are many ways to estimate the flux linkage in d- and q-axis, depending on the available input variables. In the AM the flux density in the air gap is available, thus it will be used as the input variable for the flux linkage estimation.

The flux linkage in the d- and q-axis is estimated directly by integrating the flux density over the air gap surface in specific intervals. Integration path interval is always equal to the pole pitch. Fluxes in the d- and q-axis can be estimated as:

$$\phi_d = \int_{\overline{q}-axis}^{q-axis} B_g(\theta_r)\frac{DL_{stk}}{2}d\theta_r \tag{8}$$

$$\phi_q = \int_{\overline{d}-axis}^{d-axis} B_g(\theta_r)\frac{DL_{stk}}{2}d\theta_r \tag{9}$$

The integration limits refer to a positive and negative q-axis in case of a d-axis flux, and positive and negative d-axis in q-axis flux estimation as depicted in Fig. 3, where the negative

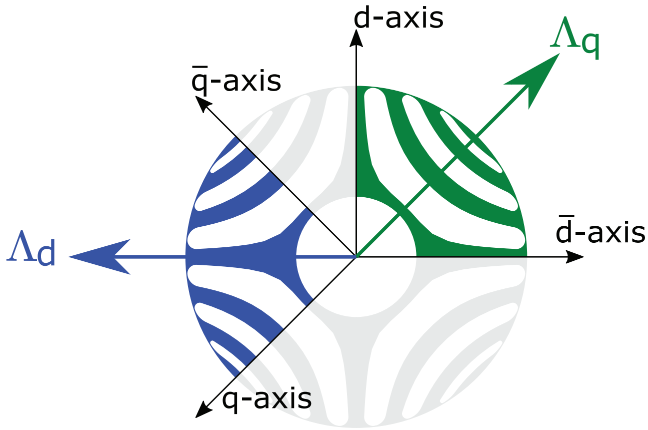

Fig. 3: Integration limits for the d- and q-axis flux linkages

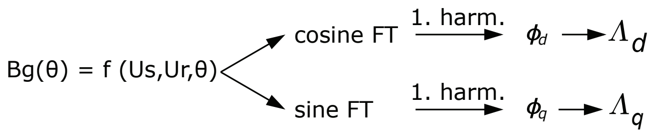

Fig. 4: Flux linkages estimation from the first harmonics coefficients

axis is labeled with the over-lined character ($\overline{d}$, $\overline{q}$). The flux linkages can be derived as

$$\Lambda_d = \frac{k_w N_s}{2}\phi_d \tag{10}$$

$$\Lambda_q = \frac{k_w N_s}{2}\phi_q \tag{11}$$

where k_w is the winding factor of the first harmonic and N_s is the number of series conductors per phase.

If the integration limits are unknown or difficult to obtain, it is possible to use simplified version of calculation only with first harmonic of the air gap flux density. The Fourier transformation is used for the first harmonic estimation, and the air gap flux density B_g is split into series of either sine and cosine functions [13]. The first cosine B_g coefficient, later referred to as $\hat{B}_{gd1}$, will be used for the d-axis flux estimation and the first sine B_g coefficient, later referred to as $\hat{B}_{gq1}$, for the q-axis flux estimation, as shown in Fig. 4.

The magnetic flux can be estimated, with known first harmonics coefficients, by the identity of curves as depicted on Fig. 5 [14]. Then, the magnetic flux can be derived as an area below a curve multiplied by the stack length.

$$\phi = \frac{2}{\pi}\hat{B}_1\frac{\pi D}{2\,p}L_{stk} = \frac{\hat{B}_1 DL_{stk}}{2\,p} \tag{12}$$

Combining the magnetic flux from (12) with the correct flux density coefficient and (10) and (11) the flux linkages become:

$$\Lambda_d = \frac{k_w N_s DL_{stk}\hat{B}_{gd1}}{4p} \tag{13}$$

$$\Lambda_q = \frac{k_w N_s DL_{stk}\hat{B}_{gq1}}{4p} \tag{14}$$

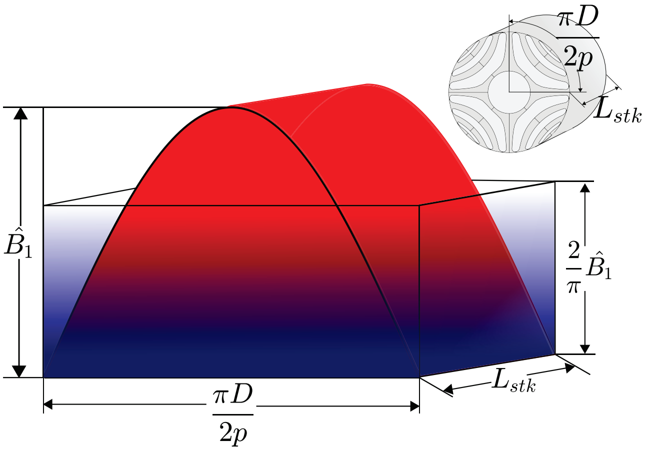

Fig. 5: Magnetic flux estimation from the sine function

Alternatively, it is also possible to obtain the magnetic flux, thus the flux linkage from the stator magnetic vector potential difference between the positive and negative axis used in the flux density integration. Combining (8) with (10) and (9) with (11) and adapting the difference potential method, the equations for d- and q-axis flux linkages become:

$$\lambda_d = \frac{k_w N_s}{2}(A_{zq} - A_{z\bar{q}})L_{stk} \tag{15}$$

$$\lambda_q = \frac{k_w N_s}{2}(A_{zd} - A_{z\bar{d}})L_{stk} \tag{16}$$

It is important to note that methods used above to estimate the flux in d- and q-axis do not consider the flux leakage phenomenon.

In case of FEA, where the phase flux linkages Λ_a, Λ_b and Λ_c are estimated integrating the vector magnetic potential across the slot area cross sections, Park transformation can be applied [14]. This method considers the leakage flux in the flux linkage computation.

(17)
$$\lambda_d = \frac{2}{3}\left[\lambda_a \cos\left(\theta_m^e\right) + \lambda_b \cos\left(\theta_m^e - \frac{2}{3}\pi\right) + \lambda_c \cos\left(\theta_m^e - \frac{4}{3}\pi\right)\right]$$

(18)
$$\lambda_q = \frac{2}{3}\left[\lambda_a \sin\left(\theta_m^e\right) + \lambda_b \sin\left(\theta_m^e - \frac{2}{3}\pi\right) + \lambda_c \sin\left(\theta_m^e - \frac{4}{3}\pi\right)\right]$$

Cross-saturation effect

The Cross-Saturation Effect (CSE) is caused by the iron non-linear behavior and is found in every electric machine. In SynRel machines there is a high CSE due to the high saturation of the rotor paths (necessary to achieve high motor torque). In addition, if iron ribs are considered, it leads to higher coupling between d- and q-axis fluxes [14]. Due to this effect, the inductance of each axis is not only a function of the current in the corresponding axis, but also of the other one [15]. Fig. 6 illustrates the ribs influence on saturation effect in SynRel machines. The thicker the ribs, the more influenced the CSE.

In the CSE comparison it is essential to compare the flux linkages obtained by using the same procedure, thus using the same input variables. The differences can be noticeable in FEA, because the software considers the flux leakage of the winding, whereas the AM does not consider the flux leakage.

The method using integration of the air gap flux density is used for the comparison, because it automatically removes most of leakage flux. Fig. 7. shows the estimated d- and q-axis fluxes by the AM and FEA. Table 2 reports comparison of the computation times. It can be noted that the analytical model produces quite accurate results overall. Only the knee on the d-axis flux linkage appears sharper with higher values.

With the estimated d- and q-axis flux linkages with given currents $\Lambda_d(I_d, I_q)$ and $\Lambda_q(I_d, I_q)$ it is possible to derive the torque and the voltage limit ellipses.

$$T = \frac{3}{2}p[\Lambda_d I_q - \Lambda_q I_d] \tag{19}$$

$$\frac{V_N}{\omega} \approx \Lambda = \sqrt{\Lambda_d^2 + \Lambda_q^2} \tag{20}$$

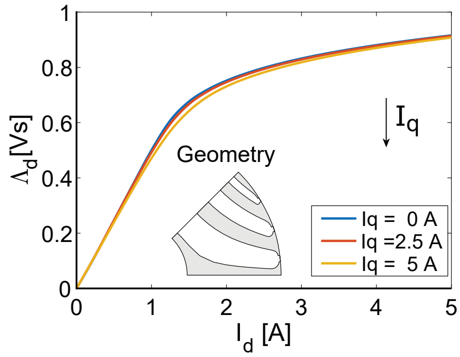

(a) *Model without ribs*

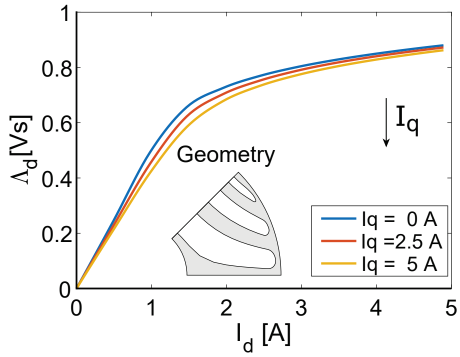

(b) *Model with outer ribs*

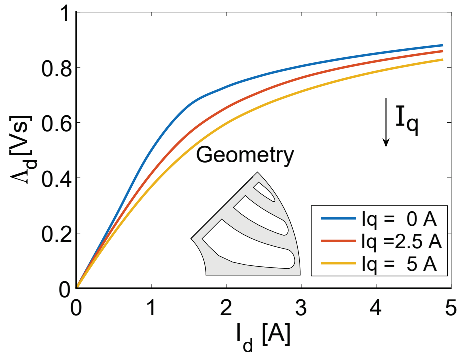

(c) *Model with outer and radial ribs*

Fig. 6: Rib influence on the cross-saturation

Table 2: Comparison of saturation calculation time

Calculation type	Current step [A]	Time [s]
FEA	0.25	16213
	0.5	4891
AM	0.25	609
	0.5	220

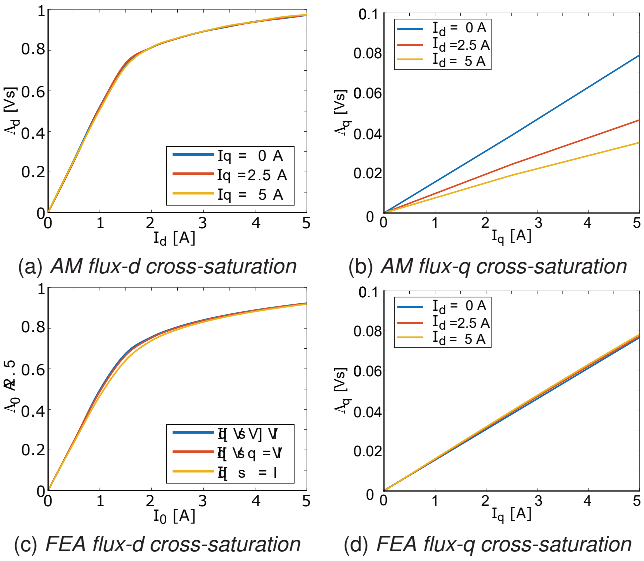

(a) *AM flux-d cross-saturation* (b) *AM flux-q cross-saturation*

(c) *FEA flux-d cross-saturation* (d) *FEA flux-q cross-saturation*

Fig. 7: AM and and FEA comparison

Table 3: Comparison of variables

Variable	FEA	AM	Difference [%]
Max MTPA torque	9.9	11	11.1
Max speed	20 543	20 141	-1.957
MTPV	10 050	11 203	11.5

where I_d and I_q are d- and q-axis currents. From the current and voltage limits, torque vs. speed, power vs. speed and current vs. speed characteristics can be derived. In Fig. 8 all of these characteristics were obtained and compared with FEA results. The results obtained by the AM are very similar to the FEA results. Comparing Fig. 8 (a) and (b) it can be observed that the MTPA trajectory is correectly identified by the AM, both in linear condition (near the origin where the current angle is $45°$) and in nonlinear ase (especially the base point along the current limit circle). Such and accuracy is due to the perfect agreement between the constant-torque contours shape, despite the fact, that the torque overestimated analytically. Comparing the other plots in Fig. 8, it is evident that the analytical model accurately predicts the base speed, the power at 20 krpm, while it overestimates the MTPV initial speed (at around 20 krpm). This may be due to a slightly higher d-axis inductance for the AM, which leads to a slightly higher MTPV current angle (see Fig. 8(a) and (b)), or to the fact that FE also consideres the leakage flux which becomes relevant at low currents. Especially considering the calculation time of the whole procedure, which is 22 times lower in case of 0.5 A current step and almost 27 times lower in case of 0.25 A current step, the analytical model becomes a very promising tool for the rapid estimation of a motor performance. The the difference between FEA and AM calculations can be seen in the table 3. Difference is reasonable, if the time needed for estimation is taken into account. Therefore the AM can deliver reasonably satisfactory results, if the convergence settings are properly set.

Conclusion

This paper presented and extended a commonly used analytical model to consider cross-saturation effect and to map the (i_d, i_q) plane of synchronous reluctance machines. An overview of various methods for the d- and q-axis flux linkages estimation has been shown. The comparison of saturation effect showed, that in the analytical model the d-axis

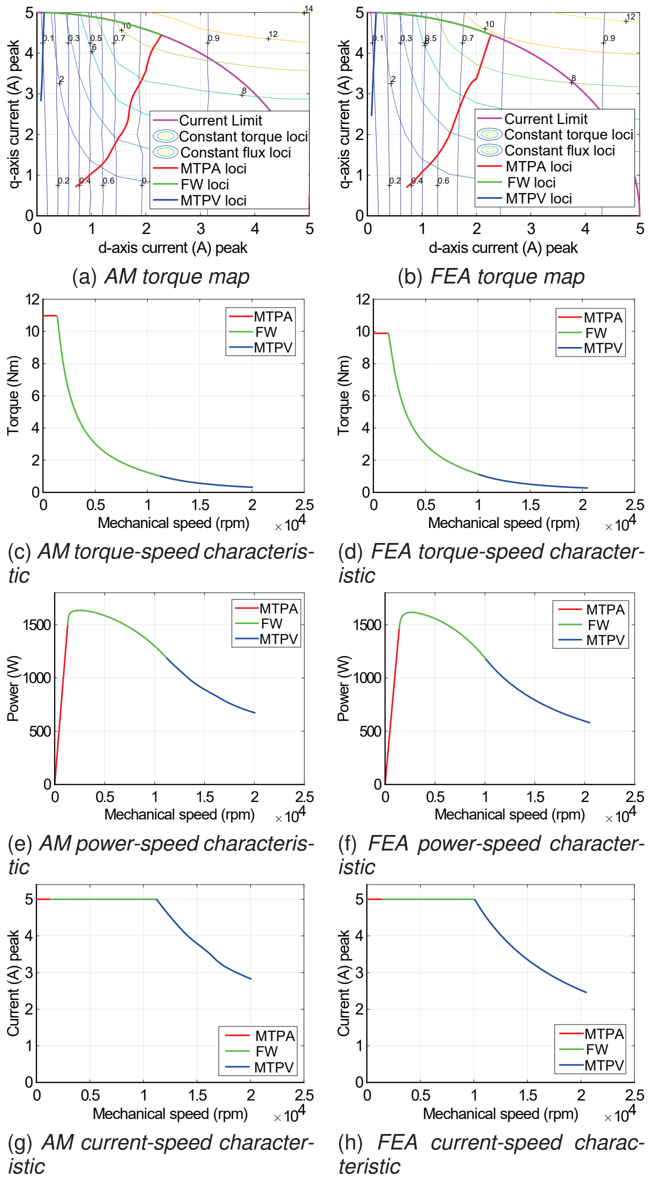

(a) *AM torque map* (b) *FEA torque map*

(c) *AM torque-speed characteristic* (d) *FEA torque-speed characteristic*

(e) *AM power-speed characteristic* (f) *FEA power-speed characteristic*

(g) *AM current-speed characteristic* (h) *FEA current-speed characteristic*

Fig. 8: AM and and FEA comparison

current has a significant influence on the q-axis flux, whereas in FEA no such a behavior is found. Only the q-axis flux with the d-axis current equal to zero is worthy to compare with the FEA characteristics.

The d-axis flux linkage at the maximum current is slightly higher, with various q-axis currents. Both of the flux differences have influence on the estimated torque. Nonetheless the (i_d, i_q) mapping and the derived results are in good agreement with finite element and prove that the analytical model can be used for quick performance analysis and initial design phases, thanks to its reliability and speed.

Acknowledgment

This research was financially supported by a project of a specific research program of Brno University of Technology No. FEKT-S-17-4374 (Increasing the efficiency of electric drives).

Authors: *Ladislav Knebl and Cestmir Ondrusek are with the Faculty of Electrical Engineering and Communication, Department of Power Electrical and Electronic Engineering, Brno University of Technology, Brno 61600, Czech Republic, e-mail: ladislav.knebl@vutbr.cz. N. Bianchi and G. Bacco are* *with the Department of Industrial Engineering, University of Padova, 35131 Padova, Italy.*

REFERENCES

[1] Z. Wei, "Finite element computation of synchronous reluctance motor," in *2011 IEEE International Conference on Microwave Technology Computational Electromagnetics*, May 2011, pp. 391–394.
[2] S. Tahi and R. Ibtiouen, "Finite element calculation of the dq-axes inductances and torque of synchronous reluctance motor," in *2014 International Conference on Electrical Sciences and Technologies in Maghreb (CISTEM)*, Nov 2014, pp. 1–5.
[3] C. López, T. Michalski, A. Espinosa, and L. Romeral, "Rotor of synchronous reluctance motor optimization by means reluctance network and genetic algorithm," in *2016 XXII International Conference on Electrical Machines (ICEM)*, Sept 2016, pp. 2052–2058.
[4] P. Alotto, M. Barcaro, N. Bianchi, and M. Guarnieri, "Optimization of IPM motors with machaon rotor flux barriers," in *Digests of the 2010 14th Biennial IEEE Conference on Electromagnetic Field Computation*, May 2010.
[5] S. Stipetic, D. Zarko, and M. Kovacic, "Optimised design of permanent magnet assisted synchronous reluctance motor series using combined analytical - finite element analysis based approach," *IET Electric Power Applications*, vol. 10, no. 5, pp. 330–338, 2016.
[6] M. Degano, H. Mahmoud, N. Bianchi, and C. Gerada, "Synchronous reluctance machine analytical model optimization and validation through finite element analysis," in *2016 XXII International Conference on Electrical Machines (ICEM)*, Sept 2016, pp. 585–591.
[7] H. Mahmoud and N. Bianchi, "Nonlinear analytical model of eccentric synchronous reluctance machines considering the iron saturation and slotting effect," *IEEE Transactions on Industry Applications*, vol. 53, no. 3, pp. 2007–2015, May 2017.
[8] H. Mahmoud, N. Chiodetto, and N. Bianchi, "Magnetic field analytical computation in synchronous reluctance machines considering the iron saturation," in *IEEE Energy Conversion Congress and Exposition (ECCE)*, Sept 2016, pp. 1–8.
[9] L. Alberti, M. Barcaro, and N. Bianchi, "Design of a low torque ripple fractional-slot interior permanent magnet motor," in *IEEE Energy Conversion Congress and Exposition (ECCE)*, Sept 2012, pp. 509–516.
[10] M. Barcaro and N. Bianchi, "Torque ripple reduction in fractional-slot interior PM machines optimizing the flux-barrier geometries," in *XXth International Conference on Electrical Machines (ICEM)*, Sept 2012, pp. 1496–1502.
[11] M. Barcaro, N. Bianchi, and F. Magnussen, "Rotor flux-barrier geometry design to reduce stator iron losses in synchronous IPM motors under FW operations," *IEEE Transactions on Industry Applications*, vol. 46, no. 5, pp. 1950–1958, Sept 2010.
[12] H. Mahmoud, G. Bacco, M. Degano, N. Bianchi, and C. Gerada, "Synchronous reluctance motor iron losses: Considering machine non-linearity at MTPA, FW, and MTPV operating conditions," *IEEE Transactions on Energy Conversion*, 2018.
[13] A. Domínguez, "Highlights in the history of the Fourier transform [retrospectroscope]," *IEEE Pulse*, vol. 7, no. 1, pp. 53–61, Jan 2016.
[14] N. Bianchi and T. M. Jahns, *Design, analysis, and control of interior PM synchronous machines: tutorial course notes ; Seattle, Oct. 5, 2004*. CLEUP, 2004.
[15] J. Barral, R. Bonnefille, S. Henry, and J. Mesiere, "Contribution to the modelisation of satured synchronous machines," in *Proc. Conf. first Int. Conf. Elect. Mach.; Athens, Greece*, vol. 3, Oct. 1980, p. 1476–1484.